Solar Phys (2015) 290:2333–2353
DOI 10.1007/s11207-015-0753-5

Study of Cosmic-Ray Modulation During the Recent Unusual Minimum and Mini-Maximum of Solar Cycle 24

O.P.M. Aslam[1] · Badruddin[1]

Received: 20 January 2015 / Accepted: 28 July 2015 / Published online: 21 August 2015

Abstract After a prolonged and deep solar minimum at the end of Cycle 23, the current Solar Cycle 24 is one of the lowest cycles. These two periods of deep minimum and mini-maximum are separated by a period of increasing solar activity. We study the cosmic-ray intensity variation in relation with the solar activity, heliospheric plasma and magnetic field parameters, including the heliospheric current sheet, during these three periods (phases) of different activity level and nature: (a) a deep minimum, (b) an increasing activity period, and (c) a mini-maximum. We use neutron monitor data from stations located around the globe to study the rigidity dependence on modulation during the two extremes, *i.e.*, minimum and maximum. We also study the time lag between the cosmic-ray intensity and various solar and interplanetary parameters separately during the three activity phases. We also analyze the role of various parameters, including the current sheet tilt, in modulating the cosmic-ray intensity during the three different phases. Their relative importance and the implications of our results are also discussed.

Keywords Galactic cosmic rays · Solar modulation · Deep solar minimum · Solar wind

1. Introduction

Solar modulation of galactic cosmic rays (GCR) has been a subject of intense research, especially to assess the continuously changing behavior of the Sun and its influence on cosmic-rays. The modulation of GCR intensity associated with the $\approx$11-year solar activity cycle has been studied for the past several decades (*e.g.*, Forbush, 1954; Burlaga *et al.*, 1985; Venkatesan and Badruddin, 1990; Storini *et al.*, 1995; Sabbah and Rybansky, 2006; Kudela, 2009; Heber, 2013; Chowdhury, Kudela, and Dwivedi, 2013; and references therein). The long-term GCR modulation shows an $\approx$ 22-year cycle related to the solar magnetic cycle as the solar polarity reverses near solar maximum of every activity cycle. The polarity-dependent effects on cosmic rays are an area of active research as well (*e.g.*, Jokipii, Levy,

✉ Badruddin
badr.physamu@gmail.com

[1] Department of Physics, Aligarh Muslim University, Aligarh 202002, India

and Hubbard, 1977; Potgieter and Moraal, 1985; Smith and Thomas, 1986; Cliver and Ling, 2001; Kota, 2013; Potgieter, 2014; Laurenza *et al.*, 2014; Potgieter *et al.*, 2014; Thomas, Owens, and Lockwood, 2014; Thomas *et al.*, 2014; and references therein).

The transport of GCR particles in the heliosphere is subjected to four distinct types of modulation mechanisms: convection, adiabatic energy changes, gradient and curvature drifts, and diffusion (Kota, 2013). It has been an accepted paradigm that drifts are the dominant processes during low to moderate solar activity, while diffusion is considered to dominate the cosmic-ray modulation during solar maximum (see also Jokipii and Wibberenz, 1998; Pacini and Usoskin, 2015). However, it has been suggested that all the four basic mechanisms (convection, diffusion, adiabatic energy change, and drifts) are important, but that their relative importance varies during different phases (*e.g.*, increasing and decreasing activity, maximum and minimum) throughout the solar cycle (*e.g.*, McKibben *et al.*, 1995; McDonald, Nand, and McGuire, 1998), and there is evidence (*e.g.*, Badruddin, Singh and Singh, 2007; Singh, Singh, and Badruddin, 2008; Aslam and Badruddin, 2012, 2014) that indicates such variations. It has recently been suggested (see Potgieter, 2014) that GCR modulation is an intriguing interplay among basically four mechanisms that changes over the solar cycle and from one solar cycle to another.

The $\approx$11- and $\approx$22-year GCR intensity modulation in antiphase with solar activity shows some time lag. This time lag has been observed to be different in odd-numbered solar activity cycles (*e.g.*, Solar Cycles 21 and 23) from even-numbered solar cycles (*e.g.*, Solar Cycles 20 and 22). The time lag also differs in positive-polarity epochs (when the northern solar pole has a positive polarity, *i.e.*, an outward-directed field) from negative solar polarity epochs (when the northern solar pole has a negative polarity, *i.e.*, an inward-directed field) (*e.g.*, Mavromichalaki, Belehaki, and Rafois, 1998; Kane, 2003; Badruddin, Singh and Singh, 2007; Singh, Singh, and Badruddin, 2008; Inceoglu *et al.*, 2014; Kane, 2014). However, a number of similarities and differences in GCR intensity modulation during different phases of the solar cycle still need to be understood (*e.g.*, Potgieter, 2014; Aslam and Badruddin, 2014; Thomas, Owens, and Lockwood, 2014).

The recent solar minimum between Solar Cycles 23 and 24 was quite unusual in that is was longer and deeper, and the present maximum is the smallest since that of Solar Cycle 14. Compared to the other three minima during the space age, the recent minimum was unusual in many aspects (Jian, Russell, and Luhmann, 2011; Pacini and Usoskin, 2015). Some of these aspects are a record low interplanetary magnetic field intensity, slower solar wind, reduced solar wind dynamic pressure, and weaker solar polar magnetic fields. Cosmic-ray modulation during this peculiar minimum has been studied using ground-based neutron monitor data (*e.g.*, Heber *et al.*, 2009; Moraal and Stoker, 2010; Badruddin, 2011; Aslam and Badruddin, 2012; Cliver, Richardson, and Ling, 2013; Ahluwalia, 2014; Pacini and Usoskin, 2015), as well as spacecraft data (*e.g.*, Mewaldt *et al.*, 2010; McDonald, Webber, and Reames, 2010; Leske *et al.*, 2013; Guo and Florinski, 2014; Strauss and Potgieter, 2014), and many peculiarities have been observed. Some of these are that (a) the GCR flux was the highest of the space age, (b) the energy spectrum was softer than expected, and (c) the modulation was weaker than in the three previous minima at low-energy particles, which are recorded by high-latitude Earth-based neutron monitors at polar sites (see Aslam and Badruddin, 2012; Strauss and Potgieter, 2014; Pacini and Usoskin, 2015, and references therein).

In this work, we mainly concentrate on the two recent peculiar periods, the recent deep minimum (DeepMin) between Solar Cycles 23 and 24, and the mini-maximum (MiniMax) of Solar Cycle 24. Additionally, we consider the period of increasing solar activity between these two periods of special characteristics.

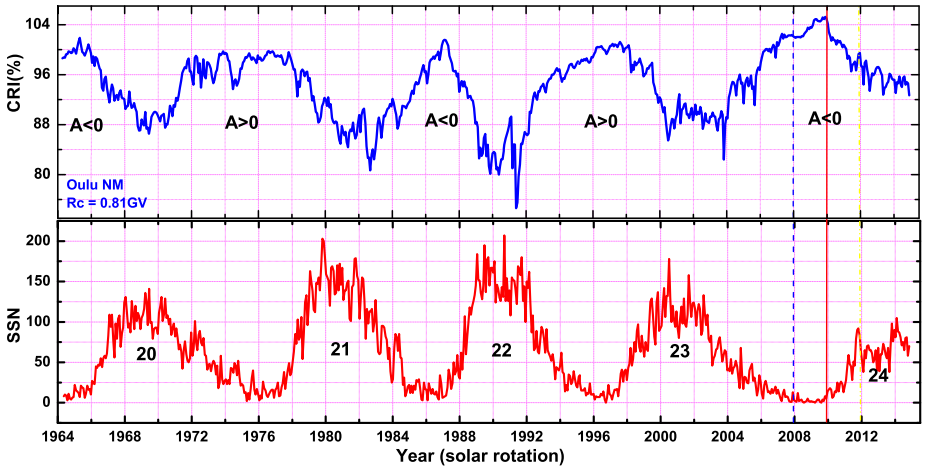

Figure 1 The variation of the relative cosmic ray intensity and solar activity (SSN) with a 27-day average from April 1964 to November 2014. The beginning of DeepMin, increasing, and MiniMax phases are indicated by vertical lines.

2. Results and Discussion

2.1. Time Variation of the GCR Intensity and Solar and Interplanetary Parameters

The cosmic-ray flux has been continually monitored for the past several decades by ground-based neutron monitors (NMs). The 27-day average cosmic-ray intensity recorded at the Oulu NM from April 1964 up to November 2014 is shown in the upper panel of Figure 1. The sunspot number is usually considered as a key indicator of solar activity because of the length of the available record. To compare the temporal variation in cosmic-ray intensity with solar activity, the lower panel of Figure 1 shows the solar rotation averaged sunspot number variation for the corresponding periods during different solar activity cycles (Solar Cycle 20 to Solar Cycle 24) and different solar polarity epochs ($A > 0$ and $A < 0$). Here A represents the polarity of the solar magnetic field, which is taken as positive ($A > 0$) when the dominant polar field is outward in the northern and inward in the southern hemisphere, and it is taken as negative ($A < 0$) if the opposite is the case of the solar polar field in the northern and southern hemispheres. The period of interest for this study (DeepMin, ascending phase, and MiniMax) are marked between the vertical lines on the right side of this figure. More specifically, the start of the DeepMin (with a blue dashed line), the ascending phase (with a red line), and the MiniMax (with a dash-dotted line) are plotted. All the three phases under consideration fall into the period of negative polarity ($A < 0$) of the solar magnetic field.

These two periods are unique at least in the sense that a record-high GCR intensity was recorded during the DeepMin compared to intensities recorded during previous minima. The MiniMax is the solar maximum with the lowest sunspot number (SSN) of various solar maxima since the beginning of the space era.

To compare the three periods with variations in various parameters, we plot the GCR intensity and the SSN in Figure 2(a) for the limited period of 2006 – 2014. The varia-

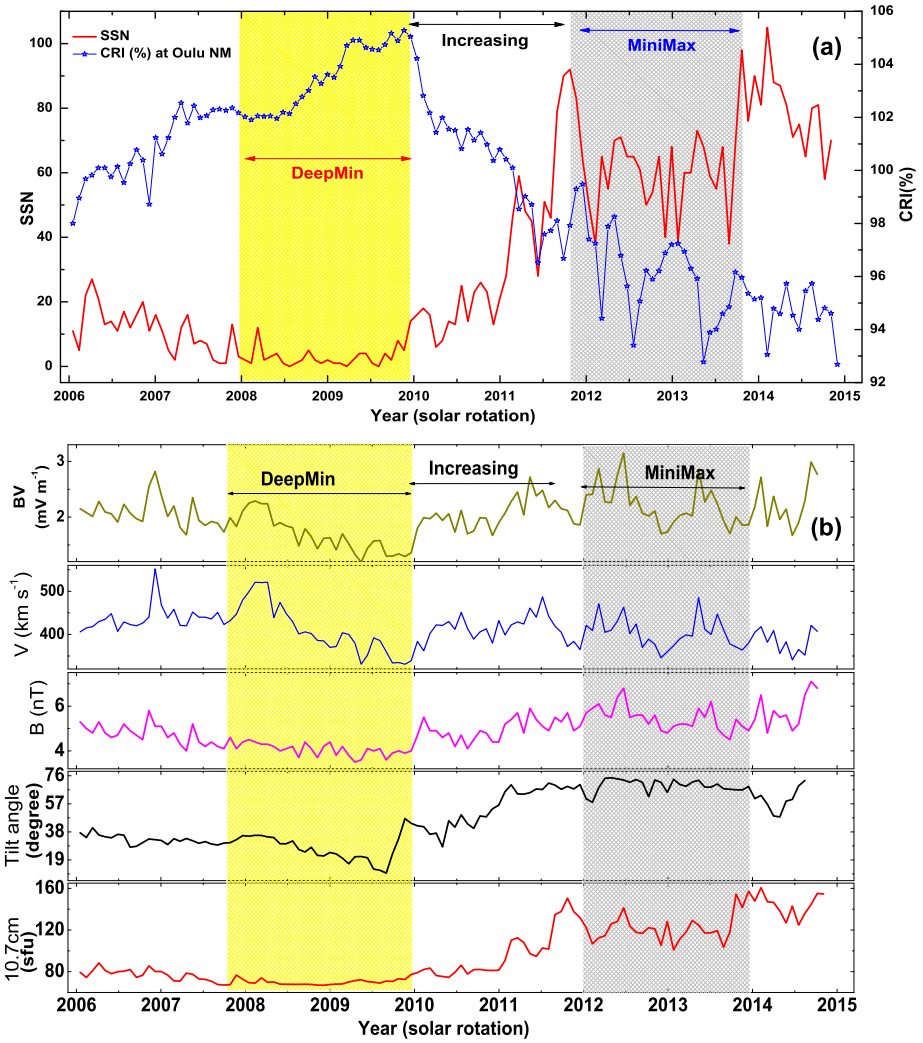

Figure 2 (a) The variation of cosmic ray intensity and solar activity (SSN) with a 27-day average from January 2006 to November 2014. The shaded portions indicate the DeepMin and MiniMax phases. (b) Variation of the 10.7 cm solar radio flux, tilt of the HCS, IMF strength (B), solar wind velocity (V), and the product BV over a solar rotation average during the period January 2006 – November 2014. The shaded portions indicate the DeepMin and MiniMax phases.

tion of the solar wind parameters, the velocity V ($\mathrm{km\,s^{-1}}$), the magnetic field B (nT), and the electric field BV ($\mathrm{mV\,m^{-1}}$) along with the tilt of the heliospheric current sheet (degree) and the 10.7 cm solar radio flux (sfu) are shown in Figure 2(b) for the period 2006 – 2014 averaged over a solar rotation. The period of DeepMin and MiniMax are shaded. The 10.7 cm solar radio-flux variation is similar to the SSN, *i.e.*, after the DeepMin of 2009 it reached a peak at the end of 2011 and, after a decrease, it maintained a lower level, although fluctuating, for a period of about two years. This period is marked as MiniMax and has a duration of 25 solar rotations (24 October 2011 to 29 Au-

gust 2013). To compare the statistical analysis results of the three solar activity phases, we took the same duration for the three phases. Thus, 25 solar rotations just before the end of the deep solar minimum between Solar Cycles 23 and 24 as DeepMin (20 December 2007 to 25 October 2009) and 25 solar rotations after the deep solar minimum as ascending phase (21 November 2009 to 27 September 2011) were considered for the analysis. The tilt angle reached a lowest value of 10.1 degree in the DeepMin (October 2009), and then it started to increase. During the MiniMax period, the tilt angle was around 70 degree, which is almost similar to the tilt angle reached during the previous three maxima. The interplanetary magnetic field reached its lowest level during the DeepMin between Solar Cycles 23 and 24 (3.5 nT averaged over a solar rotation), and it gradually started to increase along the last solar rotations of 2009. During the MiniMax period, the interplanetary magnetic field was around 5 nT, and the magnitude and fluctuations are lower than in the same phase in previous solar cycles (see Aslam and Badruddin, 2014; Ahluwalia and Ygbuhay, 2015). The solar-rotation-averaged solar wind velocity reached a low value in 2009 (331 $\mathrm{km\,s^{-1}}$), rose to a level of about 450 $\mathrm{km\,s^{-1}}$, and afterward stayed at a relatively low value, fluctuating around $\approx$400 $\mathrm{km\,s^{-1}}$ during the MiniMax.

The upper panel of Figure 2(b) shows the temporal variation of the interplanetary electric field ($E = BV$) averaged over a solar rotation for the period 2006 – 2014. The electric field reached a very low level in 2009 (1.2 $\mathrm{mV\,m^{-1}}$), and gradually increased to $\approx$3 $\mathrm{mV\,m^{-1}}$ during the MiniMax, but this level is lower than in similar phases of previous solar cycles (see Aslam and Badruddin, 2014).

2.2. Time Lag Between GCR Intensity and Solar and Interplanetary Parameters During DeepMin, MiniMax, and the Ascending Phases of Solar Cycle 24

We can observe in Figure 2 that there appears to be a shift in the occurrence of *peaks and dips* in GCR intensity changes and some of the solar and interplanetary parameters due to a possible time lag between them. To determine the time lag between the GCR intensity and solar and interplanetary parameters, we considred the three phases with equal duration (25 solar rotations, $\approx$ two years). We calculated the Pearson correlation coefficients between the GCR intensity and other parameters for a range of time lags from -5 to $+30$ solar rotations. The correlation coefficients so obtained are plotted in Figures 3 and 4. We can infer the most probable time lag between the GCR intensity and the individual parameters from the optimum values of the correlation coefficients. The left column of Figures 3 and 4 shows the variations in the time lag correlation coefficients of various solar and interplanetary parameters during the deep minimum between Solar Cycles 23 and 24, the central column shows the variations of correlation coefficients during the increasing phase of Solar Cycle 24, and the right column shows the variations of correlation coefficients during the MiniMax phase. We observe that the time lag is different for solar parameters (SSN and 10.7 cm solar radio flux) and the tilt angle (Λ) during the three phases of solar activity, but for the solar wind parameters, the time lag is almost zero in all three phases of solar activity averaged over a solar rotation period. The zero time lag for solar wind parameters (interplanetary magnetic field, IMF strength, and solar wind velocity) is surprising because the solar wind magnetic field is known to play an important role in GCR intensity modulation. However, previous studies (*e.g.*, Chowdhury, Kudela, and Dwivedi, 2013) have also reported a zero time lag between IMF and GCR during Solar Cycle 23. One possibility, as proposed by Chowdhury, Kudela, and Dwivedi (2013), is that the local disturbances such as propagating shocks and coronal mass ejections dominate the effects of distant merged interaction regions

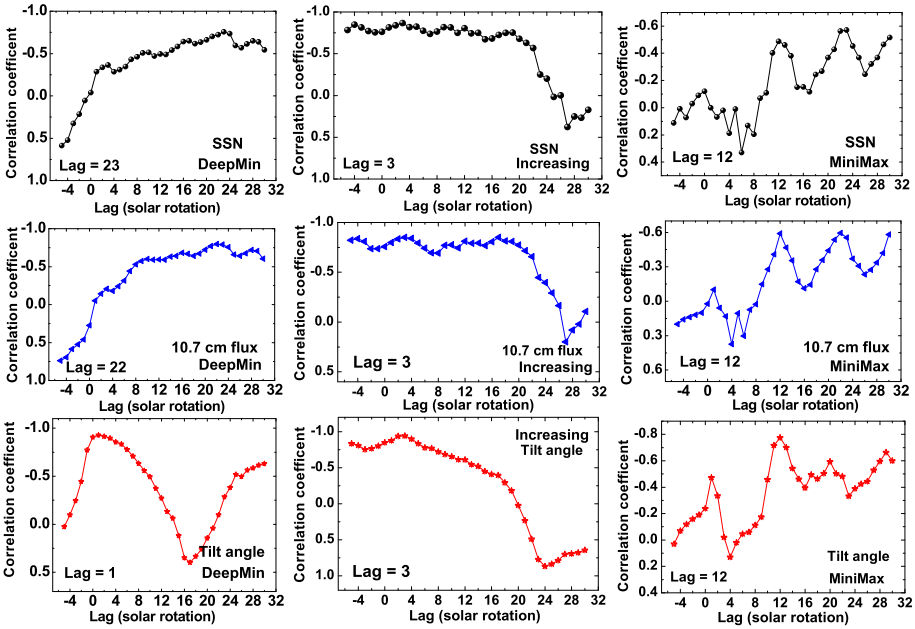

Figure 3 The variation of time lag correlation between the 27-day averaged GCR intensity and sunspot number (top three panels), GCR intensity and 10.7 cm solar radio flux (middle three panels) and GCR intensity and HCS tilt angle (three bottom panels) during DeepMin (left column), increasing (middle column), and MiniMax (right column) phases.

(MIRs) at 1 AU and the effects of Global Merged Interaction Regions (GMIRs) at large distances during this period. However, a more detailed analysis is required to clarify this. During the deep minimum, the time lag profile of the HCS tilt is quite different from the profile of SSN and 10.7 cm solar radio flux, but during the increasing and MiniMax phases, all the three profiles show similar time lag variation. As given in Table 1, the time lags for SSN and 10.7 cm solar radio flux are $\approx$22 rotations during the deep minimum, $\approx$3 rotations during the increasing phase, and $\approx$12 solar rotations during the MiniMax phase of Solar Cycle 24. In other words, the time lag between GCR intensity and solar parameters (SSN and 10.7 cm solar radio flux) is not the same during the three phases; it is shorter (3 solar rotations) during the increasing phase, intermediate (12 solar rotations) during the MiniMax, and longer ($\approx$22 solar rotations) during the DeepMin phases. The time lag for the tilt angle during DeepMin is only one solar rotation against $\approx$22 solar rotations for SSN and 10.7 cm solar radio flux during the same period. The time lag is the same for tilt angle, SSN, and 10.7 cm solar radio flux during the increasing (3 solar rotations) and MiniMax (12 solar rotations) phases. However, the lag between GCR intensity and solar wind parameters, solar wind velocity (V), IMF (B), and interplanetary electric field (BV) is found to be zero averaged over a solar rotation during all three phases, DeepMin, ascending phase, and MiniMax. A peculiar observation during MiniMax is that the time lag correlation shows some sort of periodic behavior from a negative to a positive correlation between GCR intensity and interplanetary parameters (V, B, and BV). The second peak with a negative correlation coefficient after zero time appears at $\approx$16 – 18 solar rotations ($\approx$1.3 year), a periodicity observed in the IMF and solar wind (Mursula and Vilppola, 2004) and several

Table 1 Time lag (in solar rotations) during the three studied phases for solar and interplanetary parameters calculated for GCR intensity observed at NM stations with different cutoff rigidities (R_c) and median energies (E_m). MIN, INC, and MAX correspond to DeepMin, increasing phase, and MiniMax.

NM stations	R_c (GV)	E_m (GeV)	SSN			10.7 cm flux (sfu)			Λ (degree)			B (nT)			V (km s^{-1})			BV (mV m^{-1})		
			MIN	INC	MAX	MIN	INC	MAX	MIN	INC	MAX	MIN	INC	MAX	MIN	INC	MAX	MIN	INC	MAX
McMurdo	0.01	10.122	19	3	12	20	2	12	0	2	12	0	1	0/13	0	1	0	0	1	0/14
Inuvik	0.18	10.151	23	3	12	20	3	12	1	3	12	0	1	0/19	0	1/3	0	0	1	0/16
Oulu	0.81	10.302	23	3	12	22	3	12	1	3	12	0/6	1	0/18	0	1	0	0	1	0/16
Moscow	2.46	11.030	22	1	12	22	1	12	−1	3	12	0/3	1	0/18	0	1/3	0	0	1	0/16
Irkutsk	3.66	11.858	23	1	13	21	3	12	0	2	12	0	0/5	0/13	−1	1/3	0	0	1	0/16
Jungfraujoch	4.48	12.570	24	3	12	21	2	12	1	3	11	0/5	1	0/13	1	1	0	2	1	0/16
Hermanus	4.9	12.980	23	3	12	21	3	12	1	3	12	0/6	1	0/18	2	1	0	2	1	0/16
Rome	6.32	14.596	20	3	12	20	3	12	−1	3	11	0/6	1	1	0/3	1	0	0/3	1	0/16
Potchefstrom	7.3	15.918	23	3	12	23	2	12	0	2	11	0	1	0/13	1	1	0	0	1	0
Athens	8.72	18.131	20	3	14	20	3	22	1	2	11	0	1	0/13	1	−1	0	0	1	0/16
Tsumeb	9.29	19.120	21	2	11	21	2	12	0	2	11	2	1	1	0	1	0	0	1	0
Mexico	9.53	19.553	23	3	11	20	3	12	2	2	11	0/6	1	0/18	4	1	0	0/5	1	0/16
Tibet	14.1	29.727	23	3	11	22	4	10	1	3	12	0/6	1	1	1	1	0	1	1	1
THAI	17.1	38.398	23	3	11	20	3	10	1	3	11	0	1	1	1	1	0	1	1	0

solar parameters (*e.g.*, see Cho, Hwang, and Park, 2014; Deng *et al.*, 2015; and references therein).

2.2.1. *Observation of 27-day Recurrence in the Time Lag Between GCR Intensity and Solar and Interplanetary Parameters During DeepMin*

In addition to studying the time lag over the solar rotation average scale, we also calculated the time lag correlation using daily data during DeepMin, increasing phase, and MiniMax periods (Figures 5, 6, and 7). In addition to corroborating the general shape of the lag-correlation graph shown in Figures 3 and 4, we observe interesting periodicities in the correlation between GCR and various parameters (SSN, 10.7 cm solar radio flux, V, B, and BV) during DeepMin. The 27-day periodicity in the time lag correlations of all five plots are shown in Figure 5. In addition to the 27-day periodicity, two more peaks (at ≈ 9 days and ≈ 18 days) are seen in the top three plots of Figure 5. These may be harmonics of the 27-day periodicity. To illustrate this point further, we plot an expanded version of Figure 5 for some days (see Figure 8). The 27-day periodicity (and possibly its harmonics) in the time lag plots of GCR with V and GCR with B is more clearly visible in Figure 8, in addition to the 27-day periodicity in GCR with SSN. Another important point to be noted from these plots is that the 27-day peaks occur two to three days later in the GCR with B plot and six to eight days later in the GCR with SSN plot as compared to the GCR with V plot (in the latter case peaks occur at 0, 27, 54, *etc.* days).

2.3. Dependence of GCR Modulation on Solar and Interplanetary Parameters During DeepMin, Ascending, and MiniMax Phases of the Solar Cycle

The transport of cosmic rays in the heliosphere is described by Parker's (1965) transport equation:

$$\frac{\partial f}{\partial t} = -\boldsymbol{V}.\nabla f - \boldsymbol{V}_d.\nabla f + \nabla.(K_s.\nabla f) + \frac{1}{3}(\nabla.\boldsymbol{V})\frac{\partial f}{\partial \ln P}.$$

In this expression, the four terms on the right-hand side represent each basic mechanism of cosmic ray modulation, *i.e.*, solar wind convection ($\boldsymbol{V}.\nabla f$), drifts ($\boldsymbol{V}_d.\nabla f$), diffusion ($\nabla.(K.\nabla f)$) and adiabatic energy change ($\frac{1}{3}(\nabla.\boldsymbol{V})\frac{\partial f}{\partial \ln P}$). Here f is the cosmic ray distribution function, V is the solar wind velocity, P is the rigidity, t is time, V_d is the particle drift velocity, and K_s is the symmetrical diffusion tensor.

In the above transport equation, the outward convection by the solar wind velocity ($\boldsymbol{V}$), the adiabatic energy change depending on the sign of the divergence of $\boldsymbol{V}$, the diffusion caused by turbulent irregularities in the heliospheric magnetic field ($\boldsymbol{B}$) gradient, and the curvature and current sheet drifts sensitive to the tilt of the current sheet (Λ) in the global heliospheric magnetic field directly or indirectly depend on the heliospheric parameters V, B, and Λ (see Heber, 2013; Potgieter, 2014). The GCR intensity varies in antiphase with the solar activity parameters, *e.g.*, sunspot number and 10.7 cm solar radio flux. Thus, the study of the relationship between changes in GCR intensity and various solar (SSN and 10.7 cm solar radio flux) and heliospheric parameters (V, B, Λ), especially the time delay (shorter or longer), dependence (stronger or weaker), and variation (faster or slower) between GCR intensity and various solar and heliospheric parameters (SSN, 10.7 cm solar radio flux, V, B, and Λ) during different phases of the solar cycle is expected to provide an indication about their relative importance and, consequently, about the physical process involved and their relative contribution.

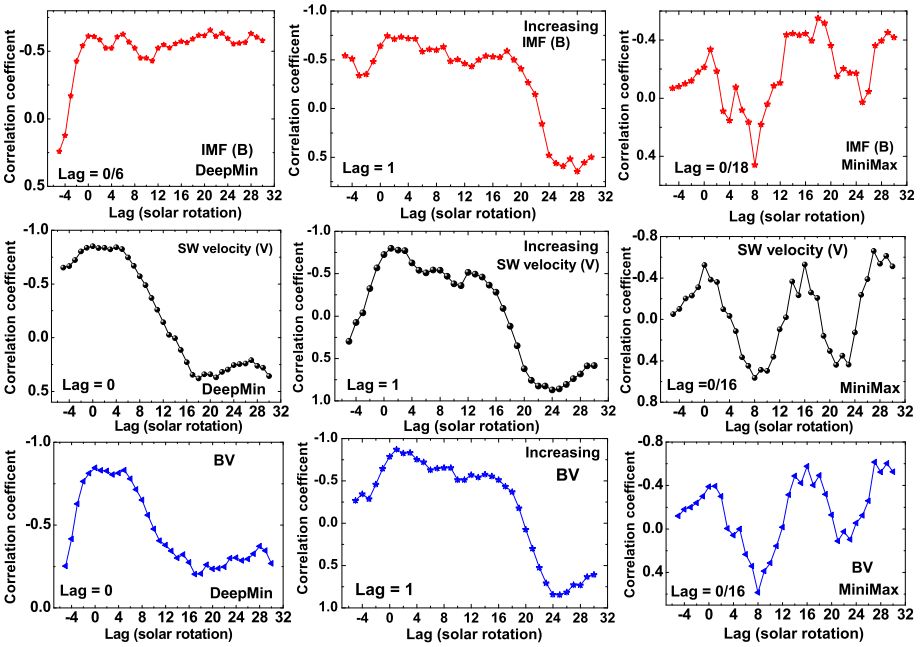

Figure 4 The variation of the time lag correlation between the 27-day averaged GCR intensity and interplanetary magnetic field (B) (top three panels), GCR intensity and solar wind velocity (V) (middle three panels), and GCR intensity and BV (three bottom panels) during DeepMin (left column), increasing (middle column), and MiniMax (right column) phases.

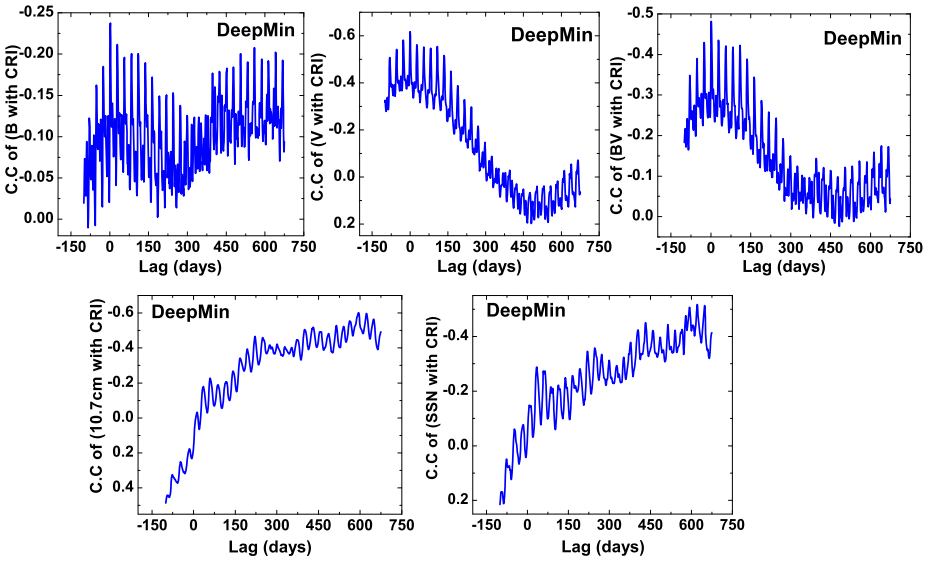

Figure 5 The variation of the time lag correlation between the daily GCR intensity and solar and interplanetary parameters (10.7 cm solar radio flux, SSN, B, V, and BV) during the DeepMin phase.

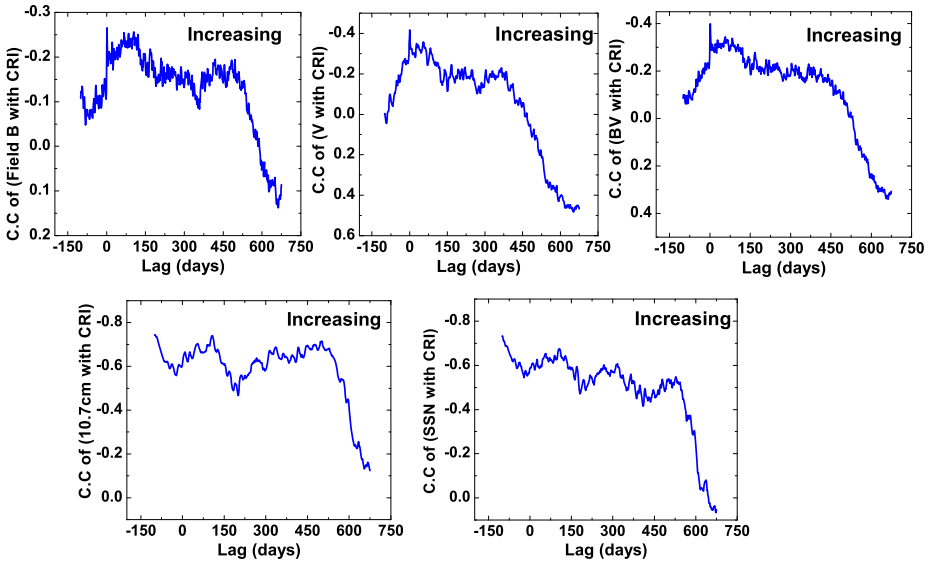

Figure 6 The variation of the time lag correlation between the daily GCR intensity and solar and interplanetary parameters (10.7 cm solar radio flux, SSN, B, V, and BV) during the increasing phase.

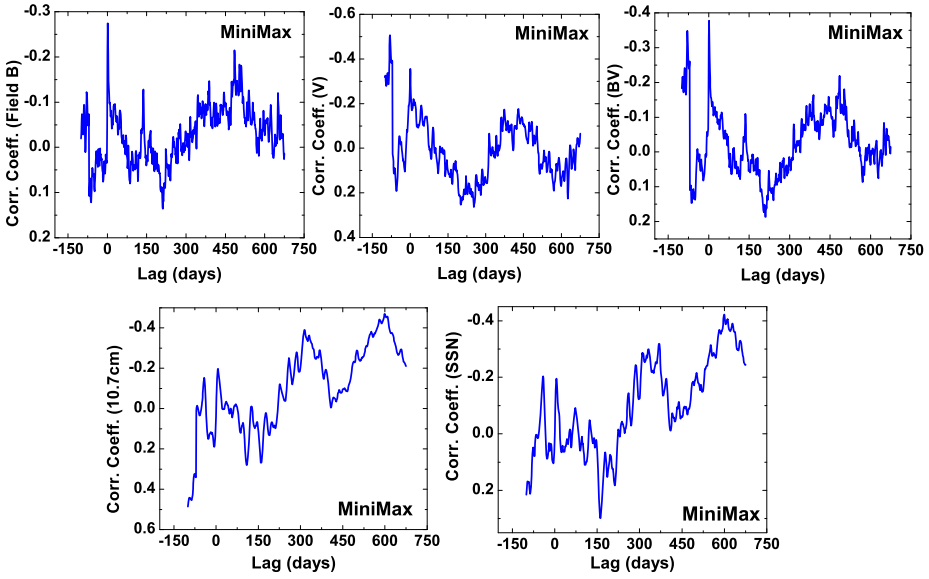

Figure 7 The variation of the time lag correlation between the daily GCR intensity and solar and interplanetary parameters (10.7 cm solar radio flux, SSN, B, V, and BV) during the MiniMax phase.

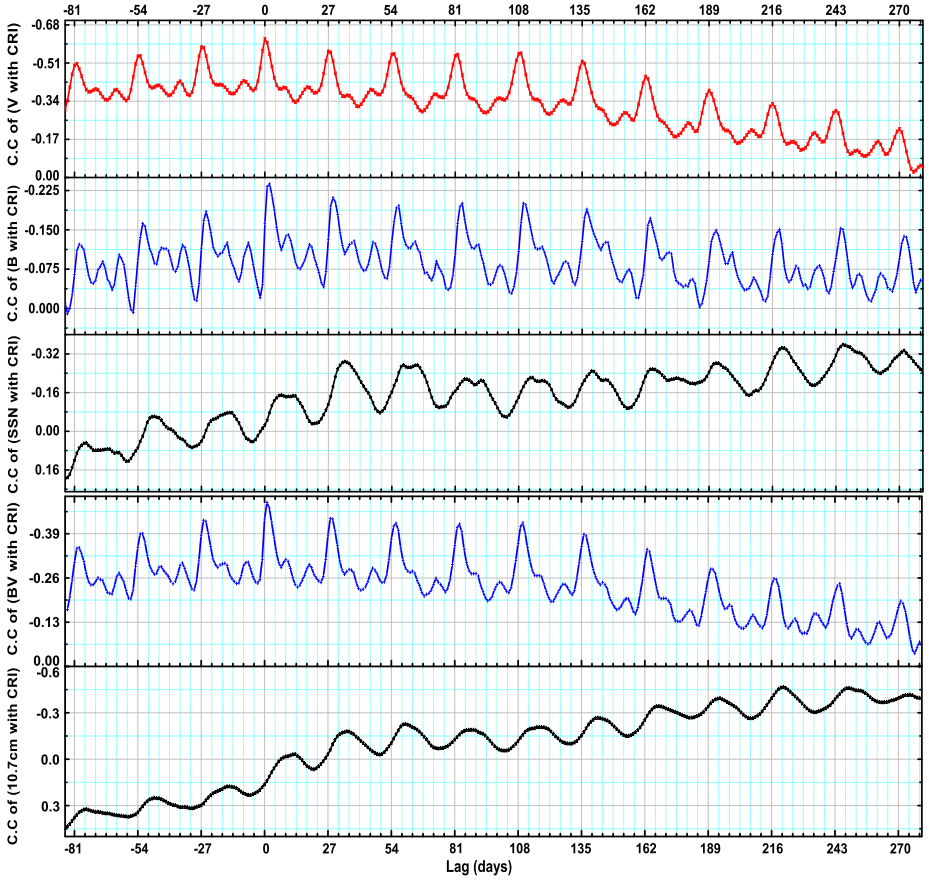

Figure 8 The periodic variation of the correlation coefficients between GCR intensity and 10.7 cm solar radio flux, *BV*, SSN, *B* and *V* during DeepMin with a daily resolution.

The best-fit value of the linear correlation coefficient obtained during the lag-time calculation of different solar and interplanetary parameters with GCR intensity observed at different ground-based NMs is tabulated in Table 2. Considering the values of the coefficients (r) as a measure of stronger (high r) or weaker (lower r) dependence of the GCR intensity modulation on the parameters, we observe that it shows a stronger dependence on solar variability (SSN and 10.7 cm solar radio flux) during the increasing phase of Solar Cycle 24 than for DeepMin and MiniMax. Similarly, the GCR modulation shows a stronger dependence on the interplanetary magnetic field (B) during the increasing phase of Solar Cycle 24. However, the dependence of GCR intensity modulation on the HCS tilt angle is stronger during both DeepMin and increasing phases than for MiniMax. But it shows a stronger dependence on the solar wind velocity during DeepMin than for MiniMax and increasing phase. Although these results are confirmed using a number of NM data with different cutoff rigidities (Table 2), interpreting them requires knowing the level of magnetic field turbulence because diffusion and drift coefficients are sensitive to this level, which varies with the solar cycle.

Strauss and Potgieter (2014) examined the drift effect during 2009 that was included in DeepMin when the GCR intensity was at its record-high level. They noted that even if the

Table 2 Best-fit values of the correlation coefficient (r) between GCR intensity and various parameters during the three studied phases at NM stations with different cutoff rigidities (R_c) and median energies (E_m). MIN, INC, and MAX correspond to DeepMin, increasing phase, and MiniMax.

NM stations	R_c (GV)	E_m (GeV)	SSN			10.7 cm flux (sfu)			Λ (degree)			B (nT)			V (km s^{-1})			BV (mV m^{-1})		
			MIN	INC	MAX	MIN	INC	MAX	MIN	INC	MAX	MIN	INC	MAX	MIN	INC	MAX	MIN	INC	MAX
McMurdo	0.01	10.122	−0.739	−0.883	−0.501	−0.776	−0.874	−0.557	−0.922	−0.923	−0.76	−0.627	−0.755	−0.579	−0.903	−0.692	−0.565	−0.893	−0.845	−0.573
Inuvik	0.18	10.151	−0.746	−0.883	−0.519	−0.773	−0.872	−0.635	−0.907	−0.933	−0.766	−0.626	−0.738	−0.583	−0.855	−0.795	−0.434	−0.855	−0.865	−0.581
Oulu	0.81	10.302	−0.756	−0.868	−0.488	−0.797	−0.851	−0.591	−0.929	−0.944	−0.776	−0.625	−0.746	−0.551	−0.851	−0.8	−0.524	−0.845	−0.875	−0.576
Moscow	2.46	11.030	−0.742	−0.834	−0.505	−0.731	−0.832	−0.628	−0.839	−0.906	−0.802	−0.642	−0.793	−0.541	−0.803	−0.741	−0.49	−0.803	−0.827	−0.643
Irkutsk	3.66	11.858	−0.774	−0.887	−0.521	−0.784	−0.844	−0.659	−0.889	−0.913	−0.593	−0.657	−0.711	−0.516	0.855	−0.765	−0.569	−0.854	−0.824	−0.36
Jungfraujoch	4.48	12.570	−0.746	−0.864	−0.445	−0.767	−0.851	−0.578	−0.917	−0.925	−0.727	−0.632	−0.769	−0.415	−0.88	−0.778	−0.567	−0.875	−0.88	−0.569
Hermanus	4.9	12.980	−0.715	−0.864	−0.506	−0.786	−0.857	−0.62	−0.897	−0.929	−0.745	−0.589	−0.763	−0.511	−0.851	−0.8	−0.523	−0.831	−0.889	−0.61
Rome	6.32	14.596	−0.722	−0.871	−0.493	−0.814	−0.859	−0.586	−0.859	−0.892	−0.716	−0.6	−0.771	−0.47	−0.853	−0.781	−0.563	−0.835	−0.888	−0.549
Potchefstrom	7.3	15.918	−0.751	−0.852	−0.478	−0.779	−0.851	−0.606	−0.909	−0.919	−0.692	−0.623	−0.812	−0.434	−0.87	−0.72	−0.546	−0.864	−0.882	−0.477
Athens	8.72	18.131	−0.72	−0.487	−0.662	−0.797	−0.445	−0.73	−0.837	−0.534	−0.705	−0.598	−0.539	−0.53	−0.854	−0.61	−0.187	−0.833	−0.607	−0.457
Tsumeb	9.29	19.120	−0.724	−0.828	−0.305	−0.765	−0.838	−0.362	−0.875	−0.908	−0.556	−0.615	−0.817	−0.512	−0.912	−0.744	−0.651	−0.888	−0.893	−0.631
Mexico	9.53	19.553	−0.726	−0.836	−0.393	−0.765	−0.831	−0.515	−0.899	−0.897	−0.672	−0.601	−0.758	−0.508	−0.883	−0.755	−0.538	−0.854	−0.864	−0.567
Tibet	14.1	29.727	−0.769	−0.831	−0.476	−0.788	−0.821	−0.437	−0.928	−0.874	−0.537	−0.642	−0.755	−0.713	−0.88	−0.755	−0.47	−0.855	−0.873	−0.573
THAI	17.1	38.398	−0.726	−0.791	−0.504	−0.786	−0.792	−0.477	−0.887	−0.859	−0.493	−0.611	−0.803	−0.627	−0.882	−0.716	−0.558	−0.866	−0.872	−0.611

drift velocity ($\boldsymbol{V}_d$) was higher in 2009, the gradient in $f(\nabla f)$ was lower because of the much lower diffusion coefficient, so that the net drift effects ($\boldsymbol{V}_d.\nabla f$) were weaker. We see that the V was very low in 2009 and since ∇f was also lower in this period, hence the net outward convection ($\boldsymbol{V}.\nabla f$) caused by the solar wind is likely to be much reduced. This might be an additional effect responsible for the record-high GCR intensity during the deep minimum. This probably indicates that reduced outward convection by the solar wind was one of the additional causes that together with diffusion and drifts caused the record-high GCR intensity during the DeepMin phase (see also Aslam and Badruddin, 2012).

2.4. Energy Dependence of the Rate of Change in GCR Intensity with the Change in Solar and Interplanetary Parameters During DeepMin, MiniMax, and Ascending Phases of Solar Cycle 24

The quantitative estimates of the rate of change in GCR intensity recorded at different NMs with different solar and interplanetary parameters were evaluated using a linear regression analysis after introducing the respective time lags. The slopes of the linear fits between rotation-averaged relative GCR intensity recorded at different NMs and corresponding solar and interplanetary parameters ($\Delta I/\Delta P$) obtained during the three different phases are tabulated in Table 3a and 3b; here ΔP stands for each analyzed parameter.

The ratios of rates at which the GCR intensity changes with different solar and interplanetary parameters during two different phases was also calculated, and the values of the ratios are shown in Table 4a and 4b. This table indicates the speed of the rate of change in GCR intensity during one phase as compared to others. From Tables 3a, 3b, 4a, and 4b, we conclude that the GCR intensity decreases at a much faster rate with the change in SSN and 10.7 cm solar radio flux during DeepMin than during MiniMax, while this decrease rate is almost the same during DeepMin and MiniMax in relation to the HCS tilt angle. However, these decrease rate values during DeepMin and MiniMax are slightly higher than during the increasing phase. For the interplanetary parameters, we observe that the GCR intensity decrease with an IMF increase is faster during DeepMin than during MiniMax, while the decrease rate is almost the same in relation to the change in the solar wind velocity during DeepMin and MiniMax. However, the decrease rate in GCR intensity with the change in V is comparatively faster during the increasing phase.

We also studied whether the rate of change in GCR intensity with different parameters ($\Delta I/\Delta P$) shows a similar (or different) dependence on the energy of the particles during the three phases. After calculating the values of the median energy of the response (E_m) of different NMs (see Usoskin *et al.*, 2008), we plot $\Delta I/\Delta P$ versus E_m during the different phases. These plots are shown in Figures 9, 10, 11, 12. From these plots, we observe that in relation to the SSN, the rate of change ($\Delta I/\Delta R$) is faster with E_m increase during the increasing and MiniMax phases than during the DeepMin phase. However, the tilt angle rate of change ($\Delta I/\Delta \Lambda$) with increase E_m is slower during DeepMin than during MiniMax and increasing phases. In addition, the E_m dependence on $\Delta I/\Delta V$ and $\Delta I/\Delta B$ is not equal during the three phases; these rates of change are higher during the increasing phase than during the other two. Although a linear fit of $\Delta I/\Delta B$ versus E_m plot during MiniMax is also shown, there is large scatter in the data points. A linear curve is expected during this phase, but transient fluctuations in GCR intensity and magnetic field data during MiniMax can be responsible for the deviation from linearity.

Table 3a Rate of change in GCR intensity with different parameters ($\Delta I/\Delta P$) during different studied phases at NM stations with different cutoff rigidities (Rc) and median energies (Em). MIN, INC, and MAX correspond to DeepMin, increasing phase, and MiniMax.

NM stations	R_c (GV)	E_m (GeV)	SSN			10.7 cm (sfu)			Λ (degree)		
			MIN	INC	MAX	MIN	INC	MAX	MIN	INC	MAX
McMurdo	0.01	10.122	-0.1893 ± 0.035	-0.145 ± 0.016	-0.0591 ± 0.021	-0.2329 ± 0.0386	-0.1832 ± 0.0208	-0.0724 ± 0.0208	-0.182 ± 0.0156	-0.148 ± 0.0126	-0.1948 ± 0.0340
Inuvik	0.18	10.151	-0.1531 ± 0.027	-0.1345 ± 0.014	-0.0494 ± 0.017	-0.2201 ± 0.0368	-0.1711 ± 0.0196	-0.0665 ± 0.0165	-0.17 ± 0.016	-0.1339 ± 0.0106	-0.1935 ± 0.0331
Oulu	0.81	10.302	-0.1281 ± 0.022	-0.1279 ± 0.015	-0.0457 ± 0.017	-0.1822 ± 0.0309	-0.1615 ± 0.0204	-0.0610 ± 0.017	-0.1452 ± 0.0118	-0.1366 ± 0.0097	-0.1965 ± 0.0326
Moscow	2.46	11.030	-0.1328 ± 0.024	-0.0878 ± 0.012	-0.0479 ± 0.017	-0.1334 ± 0.0356	-0.1277 ± 0.0203	-0.0656 ± 0.0166	-0.1212 ± 0.0161	-0.1042 ± 0.0099	-0.2081 ± 0.032
Irkutsk	3.66	11.858	-0.1226 ± 0.020	-0.0847 ± 0.009	-0.0455 ± 0.018	-0.1735 ± 0.0280	-0.1306 ± 0.0188	-0.0664 ± 0.0179	-0.1276 ± 0.013	-0.1024 ± 0.0093	-0.101 ± 0.0323
Jungfraujoch	4.48	12.570	-0.122 ± 0.022	-0.1105 ± 0.013	-0.0354 ± 0.015	-0.1773 ± 0.0303	-0.1368 ± 0.0182	-0.0506 ± 0.0146	-0.1392 ± 0.012	-0.1152 ± 0.0097	-0.1835 ± 0.0354
Hermanus	4.9	12.980	-0.0997 ± 0.020	-0.0869 ± 0.010	-0.0361 ± 0.021	-0.1531 ± 0.0246	-0.1109 ± 0.0136	-0.0486 ± 0.0126	-0.1142 ± 0.0115	-0.0904 ± 0.0073	-0.14 ± 0.0256
Rome	6.32	14.596	-0.0948 ± 0.019	-0.0634 ± 0.007	-0.026 ± 0.0094	-0.1259 ± 0.0183	-0.0806 ± 0.0098	-0.0339 ± 0.10	-0.0738 ± 0.013	-0.0627 ± 0.0068	-0.1172 ± 0.0233
Potchefstrom	7.3	15.918	-0.0922 ± 0.017	-0.0576 ± 0.007	-0.0225 ± 0.0084	-0.1292 ± 0.0225	-0.0735 ± 0.0093	-0.0313 ± 0.0084	-0.1021 ± 0.0095	-0.062 ± 0.0054	-0.0991 ± 0.0211
Athens	8.72	18.131	-0.0847 ± 0.017	-0.0428 ± 0.016	-0.0326 ± 0.0076	-0.1105 ± 0.0171	-0.0491 ± 0.0206	-0.0301 ± 0.0067	-0.0781 ± 0.0104	-0.0438 ± 0.014	-0.1159 ± 0.0271
Tsumeb	9.29	19.120	-0.0785 ± 0.015	-0.0551 ± 0.008	-0.0134 ± 0.0085	-0.0974 ± 0.0167	-0.0723 ± 0.0096	-0.0163 ± 0.0086	-0.0725 ± 0.0081	-0.0626 ± 0.006	-0.0678 ± 0.0207
Mexico	9.53	19.553	-0.1094 ± 0.021	-0.0591 ± 0.008	-0.0217 ± 0.0101	-0.1600 ± 0.0275	-0.0756 ± 0.0103	-0.0299 ± 0.0102	-0.1348 ± 0.0133	-0.0625 ± 0.0063	-0.1065 ± 0.0239
Tibet	14.1	29.727	-0.0664 ± 0.011	-0.0305 ± 0.004	-0.0124 ± 0.0066	-0.0914 ± 0.0166	-0.0395 ± 0.0058	-0.0129 ± 0.0076	-0.0736 ± 0.006	-0.0334 ± 0.0038	-0.044 ± 0.0185
THAI	17.1	38.398	-0.0413 ± 0.008	-0.0214 ± 0.003	-0.0131 ± 0.0046	-0.0621 ± 0.0010	-0.0276 ± 0.0044	-0.0133 ± 0.0050	-0.0466 ± 0.005	-0.0231 ± 0.0028	-0.0358 ± 0.0129

Table 3b Rate of change in GCR intensity with different parameters ($\Delta I/\Delta P$) during different studied phases at NM stations with different cutoff rigidities (R_c) and median energies (E_m). MIN, INC, and MAX correspond to DeepMin, increasing phase, and MiniMax.

NM stations	R_c (GV)	E_m (GeV)	B (nT)			V (km s^{-1})			BV (mV m^{-1})		
			MIN	INC	MAX	MIN	INC	MAX	MIN	INC	MAX
McMurdo	0.01	10.122	-3.355 ± 0.851	-3.675 ± 0.613	-2.290 ± 0.658	-0.0234 ± 0.0023	-0.0475 ± 0.010	-0.0324 ± 0.0097	-4.1442 ± 0.43	-6.2506 ± 0.8063	-3.4192 ± 0.9986
Inuvik	0.18	10.151	-3.178 ± 0.81	-3.249 ± 0.607	-1.628 ± 0.463	-0.0211 ± 0.0026	-0.0468 ± 0.0073	-0.02 ± 0.0085	-3.7622 ± 0.4668	-5.9370 ± 0.7033	-2.7629 ± 0.7903
Oulu	0.81	10.302	-2.574 ± 0.68	-3.176 ± 0.58	-1.358 ± 0.42	-0.0173 ± 0.0022	-0.0493 ± 0.0075	-0.02387 ± 0.0079	-3.1320 ± 0.4340	-5.8093 ± 0.6557	-2.6991 ± 0.7824
Moscow	2.46	11.030	-2.310 ± 0.64	-2.867 ± 0.449	-1.350 ± 0.428	-0.0152 ± 0.0023	-0.0358 ± 0.0063	-0.02255 ± 0.0082	-2.5936 ± 0.5283	-4.6593 ± 0.6458	-3.0487 ± 0.7418
Irkutsk	3.66	11.858	-2.575 ± 0.60	-2.206 ± 0.455	-1.231 ± 0.48	-0.0161 ± 0.002	-0.0337 ± 0.0059	-0.0203 ± 0.0069	-2.9038 ± 0.36	-4.3268 ± 0.6206	-1.2350 ± 0.755
Jungfraujoch	4.48	12.570	-2.347 ± 0.69	-2.841 ± 0.482	-1.105 ± 0.494	-0.0180 ± 0.0020	-0.0415 ± 0.0068	-0.0219 ± 0.0065	-3.2327 ± 0.365	-5.0685 ± 0.5573	-2.2615 ± 0.6674
Hermanus	4.9	12.980	-2.005 ± 0.574	-2.218 ± 0.383	-0.956 ± 0.328	-0.0154 ± 0.0019	-0.0336 ± 0.0052	-0.01807 ± 0.0060	-2.4428 ± 0.353	-4.0282 ± 0.4225	-2.1713 ± 0.5758
Rome	6.32	14.596	-1.605 ± 0.458	-1.624 ± 0.273	-0.749 ± 0.287	-0.0127 ± 0.0016	-0.0237 ± 0.0039	-0.0144 ± 0.0043	-1.9244 ± 0.29	-2.9116 ± 0.3084	-1.4455 ± 0.4490
Potchefstrom	7.3	15.918	-1.892 ± 0.485	-1.588 ± 0.233	-0.682 ± 0.29	-0.0132 ± 0.0015	-0.0203 ± 0.004	-0.0124 ± 0.0039	-2.3102 ± 0.28	-2.6872 ± 0.2926	-1.0023 ± 0.3771
Athens	8.72	18.131	-1.479 ± 0.404	-1.315 ± 0.428	-1.033 ± 0.337	-0.0106 ± 0.0013	-0.0198 ± 0.0069	-0.00527 ± 0.0057	-1.7865 ± 0.242	-2.3957 ± 0.654	-1.3278 ± 0.5281
Tsumeb	9.29	19.120	-1.304 ± 0.376	-1.596 ± 0.230	-0.636 ± 0.218	$-0.00998 \pm 9.4E{-4}$	-0.02098 ± 0.0039	-0.01296 ± 0.0031	-1.7701 ± 0.2047	-2.7167 ± 0.2801	-1.1593 ± 0.2908
Mexico	9.53	19.553	-1.961 ± 0.65	-1.547 ± 0.272	-0.706 ± 0.244	-0.0178 ± 0.0019	-0.02228 ± 0.0040	-0.01379 ± 0.0042	-2.8578 ± 0.413	-2.7503 ± 0.3264	-1.4978 ± 0.4445
Tibet	14.1	29.727	-1.214 ± 0.359	-0.802 ± 0.142	-0.746 ± 0.212	-0.0094 ± 0.0014	-0.01189 ± 0.0020	-0.00694 ± 0.0020	-1.6154 ± 0.202	-1.4445 ± 0.1646	-0.8025 ± 0.3315
THAI	17.1	38.398	-0.862 ± 0.228	-0.629 ± 0.095	-0.463 ± 0.118	$-0.0062 \pm 6.8E{-4}$	-0.0081 ± 0.0016	-0.00661 ± 0.0020	-1.080 ± 0.127	-1.0643 ± 0.1218	-0.6681 ± 0.1766

Table 4a Ratio of the rate of change in GCR intensity with different parameters ($\Delta I/\Delta P$) for the different studied phases at NM stations with different cutoff rigidities (R_c) and median energies (E_m). Min, Inc, and Max correspond to DeepMin, increasing phase, and MiniMax.

NM stations	R_c (GV)	E_m (GeV)	SSN			10.7 cm flux (sfu)			Λ (degree)		
			Inc/Min	Min/Max	Inc/Max	Min/Inc	Min/Max	Inc/Max	Min/Inc	Min/Max	Inc/Max
McMurdo	0.01	10.122	1.306	3.203	2.453	1.271	3.217	2.53	1.23	1.07	1.316
Inuvik	0.18	10.151	1.138	3.099	2.723	1.286	3.31	2.573	1.27	1.138	1.445
Oulu	0.81	10.302	1.002	2.803	2.799	1.128	2.987	2.648	1.063	1.353	1.439
Moscow	2.46	11.030	1.513	2.772	1.833	1.045	2.034	1.947	1.163	1.717	1.997
Irkutsk	3.66	11.858	1.447	2.695	1.862	1.328	2.613	1.967	1.246	0.792	0.986
Jungfraujoch	4.48	12.570	1.104	3.446	3.121	1.296	3.504	2.704	1.208	1.318	1.593
Hermanus	4.9	12.980	1.147	2.762	2.407	1.381	3.15	2.282	1.263	1.226	1.549
Rome	6.32	14.596	1.495	3.646	2.438	1.562	3.714	2.378	1.177	1.588	1.869
Potchefstrom	7.3	15.918	1.601	4.098	2.56	1.758	4.128	2.348	1.647	0.971	1.598
Athens	8.72	18.131	1.979	2.601	1.314	2.251	3.671	1.631	1.783	1.484	2.646
Tsumeb	9.29	19.120	1.425	5.871	4.121	1.347	5.975	4.436	1.158	0.935	1.083
Mexico	9.53	19.553	1.851	5.041	2.724	2.116	5.351	2.528	2.157	0.79	1.704
Tibet	14.1	29.727	2.177	5.346	2.456	2.314	7.085	3.062	2.204	0.598	1.317
THAI	17.1	38.398	1.93	3.153	1.634	2.25	4.669	2.075	2.017	0.768	1.55
Mean value of ratios	–	–	1.51	3.61	2.46	1.60	3.96	2.51	1.47	1.12	1.58

Table 4b Ratio of the rate of change in GCR intensity with different parameters ($\Delta I/\Delta P$) for the different studied phases at NM stations with different cutoff rigidities (R_c) and median energies (E_m). Min, Inc, and Max correspond to DeepMin, increasing phase, and MiniMax.

NM stations	R_c (GV)	E_m (GeV)	B (nT)			V (km s^{-1})			BV (mV m^{-1})		
			Inc/Min	Min/Max	Inc/Max	Min/Inc	Min/Max	Inc/Max	Min/Inc	Min/Max	Inc/Max
McMurdo	0.01	10.122	1.095	1.465	1.605	2.03	1.385	1.466	1.508	1.212	1.828
Inuvik	0.18	10.151	1.022	1.952	1.996	2.218	0.948	2.34	1.578	1.362	2.149
Oulu	0.81	10.302	1.234	1.895	2.339	2.85	1.38	2.065	1.855	1.16	2.152
Moscow	2.46	11.030	1.241	1.711	2.124	2.355	1.484	1.588	1.796	0.851	1.528
Irkutsk	3.66	11.858	0.857	2.092	1.792	2.093	1.261	1.66	1.49	2.351	3.503
Jungfraujoch	4.48	12.570	1.21	2.124	2.571	2.306	1.217	1.895	1.568	1.429	2.241
Hermanus	4.9	12.980	1.106	2.097	2.32	2.182	1.173	1.859	1.649	1.125	1.855
Rome	6.32	14.596	1.012	2.143	2.168	1.866	1.134	1.646	1.513	1.331	2.014
Potchefstrom	7.3	15.918	0.839	2.774	2.328	1.538	0.942	1.632	1.163	2.305	2.681
Athens	8.72	18.131	0.889	1.432	1.273	1.868	0.497	3.757	1.341	1.345	1.804
Tsumeb	9.29	19.120	1.224	2.05	2.509	2.102	1.299	1.619	1.535	1.527	2.343
Mexico	9.53	19.553	0.789	2.778	2.191	1.252	0.775	1.616	0.962	1.908	1.836
Tibet	14.1	29.727	0.661	1.627	1.075	1.265	0.738	1.713	0.894	2.013	1.8
THAI	17.1	38.398	0.73	1.862	1.359	1.306	1.066	1.225	0.985	1.617	1.593
Mean value of ratios	–	–	0.99	2.00	1.98	1.95	1.09	1.86	1.42	1.54	2.09

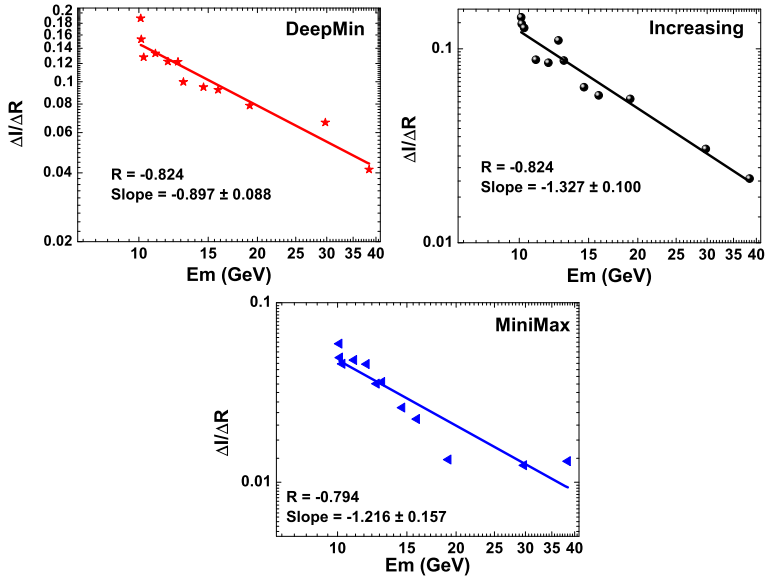

Figure 9 The variation of the rate in GCR intensity change and change in sunspot number ($\Delta I/\Delta R$) with the median energy of different stations.

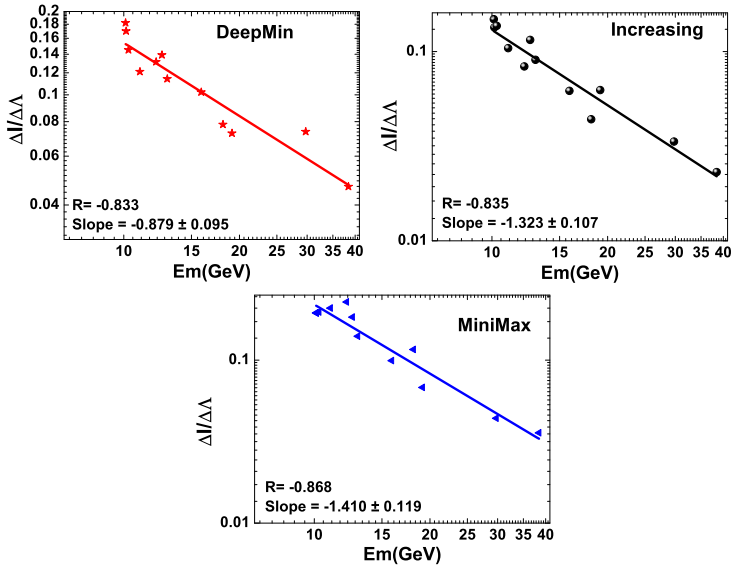

Figure 10 The variation of the rate in GCR intensity change and change in the HCS tilt ($\Delta I/\Delta\Lambda$) with the median energy of different stations.

2.5. Energy Spectrum During DeepMin and MiniMax

Using the relative change in GCR intensity with E_{m} during DeepMin and MiniMax, we studied the energy spectrum during these two peculiar periods (Figure 13). From the spec-

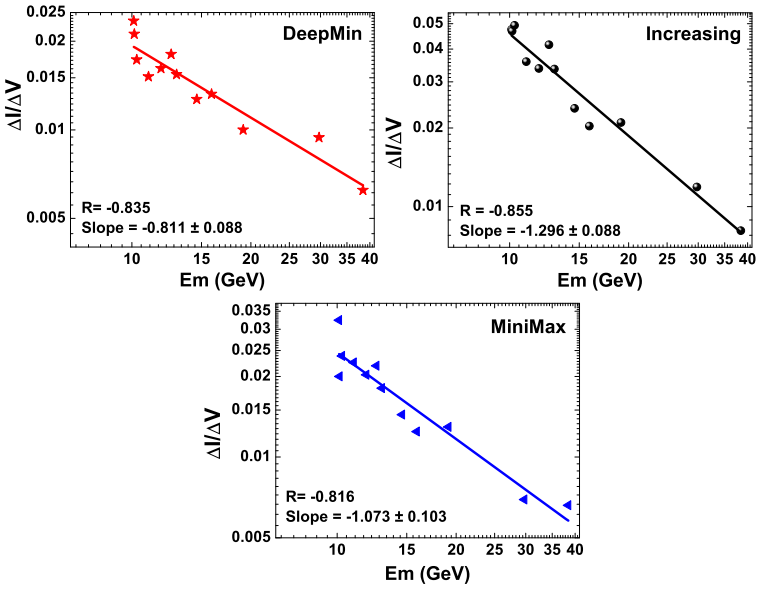

Figure 11 The variation of the rate in GCR intensity change and change in solar wind velocity ($\Delta I/\Delta V$) with the median energy of different stations.

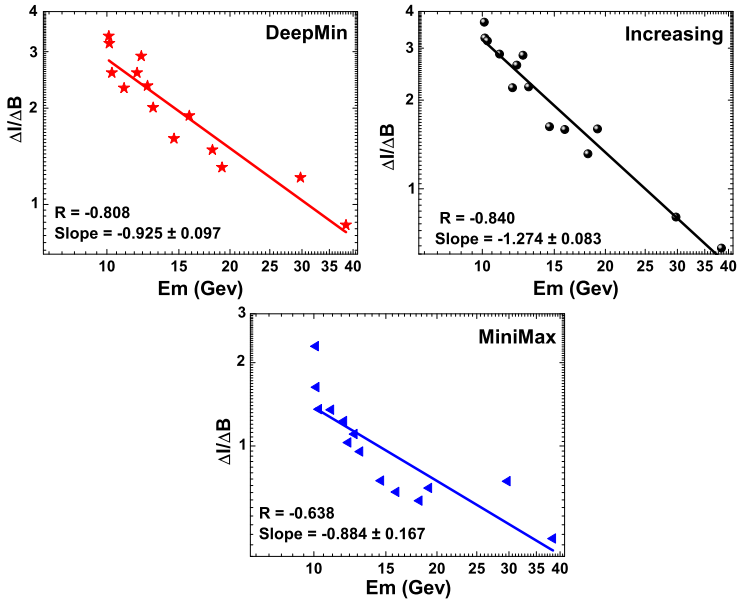

Figure 12 The variation of the rate in GCR intensity change and change in IMF strength ($\Delta I/\Delta B$) with the median energy of different stations.

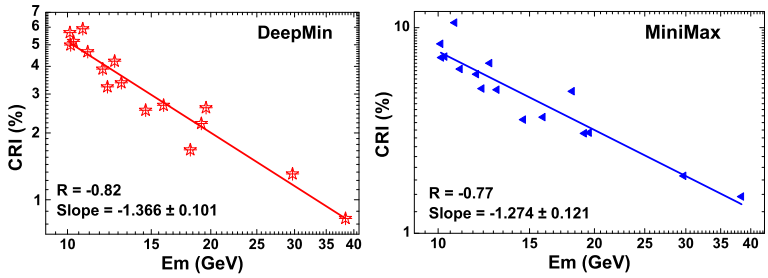

Figure 13 The energy spectrum during the DeepMin between Solar Cycles 23 and 24 and the MiniMax of Solar Cycle 24.

trum plotted using neutron monitor measurements from pole to equator, we observe almost similar energy spectra during MiniMax (exponent $\gamma = -1.27$) and DeepMin (exponent $\gamma = -1.37$).

3. Summary of Results and Conclusions

- The time lag between GCR intensity and solar parameters (SSN and 10.7 cm solar radio flux) is not the same during the three studied phases; it is shorter (3 solar rotations) during the increasing, intermediate (12 solar rotations) MiniMax and longer ($\approx$22 solar rotations) during DeepMin phases.
- Modulation of the GCR intensity shows a stronger dependence on solar variability (SSN, 10.7 cm solar radio flux) during the increasing phase of Solar Cycle 24 and a stronger dependence on solar wind velocity during DeepMin between Solar Cycles 23 and 24.
- The change in GCR intensity with the variation of solar and interplanetary plasma and field parameters and tilt angle is faster at lower cutoff rigidity stations during all the three phases of solar activity.
- The rate of GCR intensity decrease with IMF strength is faster during the DeepMin than during the MiniMax, while this rate is almost the same in relation to the change in V during DeepMin and MiniMax.
- The GCR intensity decreases at a much faster rate with the change in SSN and 10.7 cm flux during DeepMin than during MiniMax.
- The rate of GCR intensity decrease with tilt angle is almost the same during DeepMin and MiniMax.
- The energy spectrum in MiniMax is almost similar to that during DeepMin, with nearly equal values of the spectral exponent.
- The stronger or weaker relations, faster or slower changes, different energy dependence on the rate of change with different solar and interplanetary parameters during different phases suggest that the interplay among the four basic transport mechanisms changes over the solar cycle during DeepMin, MiniMax, and increasing phase of Solar Cycle 24.

Acknowledgements We thank the station managers of the neutron monitors whose data have been used in this study. Availability and use of solar and plasma and field data from the NASA/GSFC OMNI Web interface and the HCS inclination data the Wilcox Solar Observatory, Stanford, are also acknowledged. We also thank the referees, whose comments and suggestions helped us to improve the article.

References

Ahluwalia, H.S.: 2014, *Adv. Space Res.* **54**, 1704. DOI.
Ahluwalia, H.S., Ygbuhay, R.C.: 2015, *Solar Phys.* **290**, 635. DOI.
Aslam, O.P.M., Badruddin: 2012, *Solar Phys.* **279**, 269. DOI.
Aslam, O.P.M., Badruddin: 2014, *Solar Phys.* **289**, 2247. DOI.
Badruddin: 2011, In: *Proc. 32nd Int. Cosmic Ray Conf.*, SH3.5, **11**, 235. DOI.
Badruddin Singh, M., Singh, Y.P.: 2007, *Astron. Astrophys.* **466**, 697. DOI.
Burlaga, L.F., McDonald, F.B., Goldstein, M.L., Lazarus, A.J.: 1985, *J. Geophys. Res.* **90**, 12027. DOI.
Cho, I.H., Hwang, J., Park, Y.D.: 2014, *Solar Phys.* **289**, 707. DOI.
Chowdhury, P., Kudela, K., Dwivedi, B.N.: 2013, *Solar Phys.* **286**, 577. DOI.
Cliver, E.W., Ling, A.G.: 2001, *Astrophys. J.* **551**, L189. DOI.
Cliver, E.W., Richardson, I.G., Ling, A.G.: 2013, *Space Sci. Rev.* **176**, 3. DOI.
Deng, L.H., Li, B., Xiang, Y.Y., Dun, G.T.: 2015, *J. Atmos. Solar-Terr. Phys.* **122**, 18. DOI.
Forbush, S.E.: 1954, *J. Geophys. Res.* **59**, 525. DOI.
Guo, X., Florinski, V.: 2014, *J. Geophys. Res.* **119**, 2411. DOI.
Heber, B.: 2013, *Space Sci. Rev.* **176**, 265. DOI.
Heber, B., Kopp, A., Gieseler, J., Muller-Mellin, R., Fichtner, H., Scherer, K., *et al.*: 2009, *Astrophys. J.* **699**, 1956. DOI.
Inceoglu, F., Knudsen, M.F., Karoff, C., Olsen, J.: 2014, *Solar Phys.* **289**, 1387. DOI.
Jian, L.K., Russell, C.T., Luhmann, J.G.: 2011, *Solar Phys.* **274**, 321. DOI.
Jokipii, J.R., Levy, E.H., Hubbard, W.B.: 1977, *Astrophys. J.* **213**, 861. DOI.
Jokipii, J.R., Wibberenz, G.: 1998, *Space Sci. Rev.* **83**, 365. DOI.
Kane, R.P.: 2003, *J. Geophys. Res.* **108**, 1379. DOI.
Kane, R.P.: 2014, *Solar Phys.* **289**, 2727. DOI.
Kota, J.: 2013, *Space Sci. Rev.* **176**, 391. DOI.
Kudela, K.: 2009, *Acta Phys. Slovaca* **59**, 537. DOI.
Laurenza, M., Vecchio, A., Storini, M., Carbone, V.: 2014, *Astrophys. J.* **781**, 71. DOI.
Leske, R.A., Cummings, A.C., Mewaldt, R.A., Stone, E.C.: 2013, *Space Sci. Rev.* **176**, 253. DOI.
Mavromichalaki, H., Belehaki, A., Rafois, X.: 1998, *Astron. Astrophys.* **330**, 764.
McDonald, F.B., Nand, L., McGuire, R.E.: 1998, *J. Geophys. Res.* **10**, 373. DOI.
McDonald, F.B., Webber, W.R., Reames, D.V.: 2010, *Geophys. Res. Lett.* **37**, L18101. DOI.
McKibben, R.B., Connell, J.J., Lopate, C., Simpson, J.A., Zhang, M.: 1995, *Space Sci. Rev.* **72**, 367. DOI.
Mewaldt, R.A., Davis, A.J., Lave, K.A., Leske, R.A., Stone, E.C., Wiedenbech, M.E., *et al.*: 2010, *Astrophys. J. Lett.* **723**, L1. DOI.
Moraal, H., Stoker, P.H.: 2010, *J. Geophys. Res.* **115**, A12109. DOI.
Mursula, K., Vilppola, J.H.: 2004, *Solar Phys.* **221**, 337. DOI.
Pacini, A.A., Usoskin, I.G.: 2015, *Solar Phys.* **290**, 943. DOI.
Parker, E.N.: 1965, *Planet. Space Sci.* **13**, 9. DOI.
Potgieter, M.S.: 2014, *Adv. Space Res.* **53**, 1415. DOI.
Potgieter, M.S., Moraal, H.: 1985, *Astrophys. J.* **294**, 425. DOI.
Potgieter, M.S., Vos, E.E., Boezio, M., De Simone, N., Di Felice, V., Formato, V.: 2014, *Solar Phys.* **289**, 391. DOI.
Sabbah, I., Rybansky, M.J.: 2006, *J. Geophys. Res.* **111**, A01105. DOI.
Singh, M., Singh, Y.P., Badruddin: 2008, *J. Atmos. Solar-Terr. Phys.* **70**, 169. DOI.
Smith, E.J., Thomas, B.T.: 1986, *J. Geophys. Res.* **91**, 2933. DOI.
Storini, M., Borello-Filisetti, O., Mussino, V., Parisi, M., Sykora, J.: 1995, *Solar Phys.* **157**, 375. DOI.
Strauss, R.D., Potgieter, M.S.: 2014, *Solar Phys.* **289**, 3197. DOI.
Thomas, S.R., Owens, M.J., Lockwood, M.: 2014, *Solar Phys.* **289**, 407. DOI.
Thomas, S.R., Owens, M.J., Lockwood, M., Scott, C.J.: 2014, *Solar Phys.* **289**, 2653. DOI.
Usoskin, I.G., Braun, I., Gladysheva, O.G., Hörandel, J.R., Jämsén, T., Kovaltsov, G.A., *et al.*: 2008, *J. Geophys. Res.* **113**, A07102. DOI.
Venkatesan, D., Badruddin: 1990, *Space Sci. Rev.* **52**, 121. DOI.